

**Abstract.** We present optical and millimetric data for 47 intermediate Hubble type spiral galaxies located either in dense environments or in the field. We compare correlations between global parameters, such as far-infrared luminosity, blue luminosity, and total molecular gas content, with other samples of galaxies, including normal galaxies, clusters and ultraluminous infrared galaxies. We find that overall our sample is a well defined subset of these other samples of galaxies.

**Key words:** galaxy interactions-molecular gas-star formation

# Environmental effects in galaxies

## The Data<sup>\*</sup>

Duilia F. de Mello<sup>1</sup> Marcio A. G. Maia<sup>2</sup> and Tommy Wiklind<sup>1</sup>

<sup>1</sup> Onsala Space Observatory, 43992 Onsala, Sweden  
email: duilia@oso.chalmers.se, tommy@oso.chalmers.se

<sup>2</sup> Observatório Nacional, Rua Gal. José Cristino 77, RJ 20921, Brazil  
email: maia@on.br

Received; accepted

### 1. Introduction

A longstanding issue in galaxy evolution is whether galaxies evolve according to a given set of initial conditions or whether the environment in which they reside is decisive for their evolution; i.e. whether galaxy evolution depends on nature or nurture. In order to search for environmental effects in galaxies properties we have obtained optical and millimetric data for galaxies in dense regions of the Southern sky and in the field. In de Mello et al. (2001, hereafter Paper II) we present an extensive analysis of the data. The main results we found are: intermediate type spirals in dense environments have on average less molecular gas per blue luminosity, lower current SFR, the same SFE and higher atomic gas fraction when compared with field galaxies. Although none of the above results stand out as a single strong diagnostic, given their statistical significance (see Table 3 of Paper II), taken together they suggest a trend for diminished gas content and star formation activity in galaxies in high density environments. We also found that SFR per blue luminosity increases linearly as the total amount of gas increases in LINERs. This result, based on a small sample, suggests that LINERs are powered by star formation rather than an AGN. We refer to Paper II for a more detailed analysis of these results.

In this paper we present the optical and millimetric data and is organized as follows. Section 2 describes the sample, Section 3 describes the optical data, Section 4 describes the millimetric data, Section 5 describes general properties, and a comparison with other samples, Section 6 presents a summary and conclusions. A Database of optical and millimetric spectra together with digitized images are shown in Appendix A (available at <http://www.oso.chalmers.se/~duilia/env.html>).

*Send offprint requests to:* D. de Mello

<sup>\*</sup> Based on observations at the European Southern Observatory at the 15m Swedish ESO Submillimetre telescope, SEST, and at the the 1.52m telescope which is operated under the ESO-ON agreement.

### 2. Sample Selection

#### 2.1. Previous samples

Surveys of the molecular gas content in galaxies have in general been done on samples which are far-infrared selected, or galaxies selected exclusively for belonging to clusters or groups (often with a far-infrared selection criteria on top; e.g. Casoli et al. 1991, Combes et al. 1994, Leon et al. 1998). A few exceptions exist in the literature. For example, Sage (1993) presents the CO content of a distance limited sample of 65 non-strongly interacting spiral galaxies, and Horellou et al. (1995) present a CO and HI survey of spiral and lenticular galaxies in the Fornax cluster, both based on samples selected without a far-infrared criterion.

However, until now no survey of galaxies in different environments has included a rigorously selected control sample. For instance, the sample by Casoli et al. (1998) which contains a large sample of 582 objects is an important source of information concerning molecular gas in spiral galaxies. However, it was built by gathering data from various surveys and is very heterogeneous in terms of morphology and environment. It contains galaxies from several clusters as well as galaxies in the field.

#### 2.2. Dense Environment and Control Sample (HDS and CS)

In view of these biases plaguing existing samples we have selected our sample from the catalog by Maia et al. (1994) which contains objects in low and high density areas of the Southern sky. The selection of groups adopted by Maia et al. is similar to the methodology developed by Huchra & Geller (1982) with the adaptations described by Maia et al. (1989). The catalog was drawn from the ESO/Uppsala Survey of the ESO(B) Atlas (Lauberts 1982) and used velocity information from the Southern Sky Redshift Survey (e.g., da Costa et al. 1989). The groups are defined

to be formed by the accumulation of galaxy pairs with a member in common.

- The high density sample (**HDS**, hereafter) is formed by galaxies that are in groups of three or more members. They have a density contrast  $\delta\rho/\rho \geq 500$ . This is equivalent to densities larger than 18 galaxies/Mpc<sup>3</sup>. All the selected objects have radial velocities (after correction for Virgo infall) smaller than 8000 kms<sup>-1</sup>.
- The control sample (**CS**, hereafter) is made up of galaxies which are not members of any group and which are situated in regions with density contrast  $\delta\rho/\rho \leq 0.01$ , i.e. less than 0.0004 galaxies/Mpc<sup>3</sup>.

### 2.3. HDS versus Compact Groups and Poor Groups

Although a group finding algorithm was used to generate the samples, the idea is not to identify groups (either loose or compact), but galaxies in high and low local density environments. The main difference between the HDS and compact groups of galaxies is the isolation criterion which is imposed by the groups selection (Hickson 1982, Coziol et al. 2000). The only 2 compact groups (HCG 21 and HCG 90) in the region searched by Maia et al. (1994) ( $b^I \leq -30^\circ$ ,  $\delta < -17^\circ.5$ ) have 3 galaxies of each group taking part of the HDS, but none of them take part in the present subsample analysis.

The HDS should also not be confused with poor groups which are defined as systems with less than five bright galaxies but which can have 20-50 faint members (e.g, Zabludoff & Mulchaey 1998, Willmer et al. 1999). Some galaxies in these poor groups are certainly part of the HDS, but since our selection includes only members with known redshift, the HDS will have only the brighter members which have measured redshift. The HDS and CS contain in total 151 and 179 galaxies, respectively.

### 2.4. Our Subsample: Morphology selection

Maia et al. (1994) have analysed the morphology distribution of the HDS and CS and concluded that the HDS has an excess of early-type galaxies compared to the CS. This is interpreted as an effect of the morphology-density relationship (Dressler 1980); i.e. a correlation between morphological types and local density showing that the fraction of early-type galaxies increases as a function of local galaxy density while the fraction of later types decreases (see also Sanroma & Salvador-Solé 1990, Whitmore & Gilmore 1991). Since there are galaxies of all morphologies in the HDS and in the CS, the main goal of our work is to evaluate the effects of the environment in galaxies of the *same morphological type* when compared with isolated galaxies. The ideal survey would include all galaxies in the HDS and CS, however, due to large size of the samples we have imposed such a selection which is fundamental in order to avoid any bias due to the well known correlation

between morphology and physical properties of galaxies. Figures 2–4 of Roberts & Haynes (1994) summarize clearly how morphology is correlated to fundamental properties of galaxies such as, blue luminosity, far infrared luminosity, total mass, and neutral hydrogen mass. One of their conclusions is that, although the scatter is large, Sa-Sc have near constant molecular gas normalized either by the blue luminosity or by the total mass. They also pointed out that later type spirals have less molecular gas and suggest that this could also be due to the CO to H<sub>2</sub> conversion factor which would depend on morphology. Therefore, in order to have an homogeneous sample, we selected mostly intermediate spiral galaxies; i.e. Sb, Sbc, and Sc, avoiding Sa and Sd galaxies. In this work we present the analysis of the optical and millimetric data of a subsample of 47 spiral galaxies, 22 in the HDS and 25 in the CS, with velocities smaller than 5500 kms<sup>-1</sup>.

Table 1 lists information taken from the NASA/IPAC Extragalactic Database (NED) on each galaxy as follows. Column (1): designation in the ESO-Uppsala catalog (LV89); column (2): designation in other catalogs; column (3): right ascension (<sup>h m s</sup>) and declination (<sup>° ' "</sup>) for J2000; column (4): type of sample (control sample=CS and high density sample=HDS) and morphological type (Lauberts & Valentijn 1989, hereafter LV89) 1=Sa, 2=Sa-b, 3=Sb, 4=Sb-c, 5=S..., 6=Sc, Sc-d, 7=S../Irr, 8=Sd; column (5): morphological type from The Third Reference Catalogue of Bright Galaxies (RC3; de Vaucouleurs et al. 1991); column (6): number of galaxies in the same group (Maia et al. 1989); column (7): mean pairwise separation in Mpc (Maia et al. 1989); column (8): B<sub>T</sub> magnitude from RC3; column (9): IRAS 60 μm flux in Jy (Moshir et al. 1990), and column (10): IRAS 100 μm flux in Jy (Moshir et al. 1990).

## 3. The Optical Data

Long slit spectra were obtained with the Boller & Chivens Cassegrain spectrograph at the ESO 1.52m telescope (La Silla) during several runs in 1997 and 1998 as part of a key project during Brazilian time. We used the Loral/Lesser CCD (No. 39) with 2048 × 2048 pixels (1 pixel = 15 μm) and grating No. 27 which has 600 lines mm<sup>-1</sup> and gives a spectral coverage of 3600–7500 Å and dispersion of 1.7 Å pix<sup>-1</sup>. The slit width was 3'' and positioned along the major axis of the galaxies which corresponds to galactic sizes of 250 pc for the closest galaxy in the sample and to 1 kpc for the most distant galaxy in the sample.

Spectrophotometric standard stars were observed close to zenith several times during the night with a slit width of 5''. A He-Ar lamp was observed after every exposure and used for wavelength calibration. Typical exposure times were 2 × 20–30 minutes for galaxies and 5–10 minutes for stars.

Standard data reduction, including bias and flat-field correction, was performed using IRAF. One dimensional

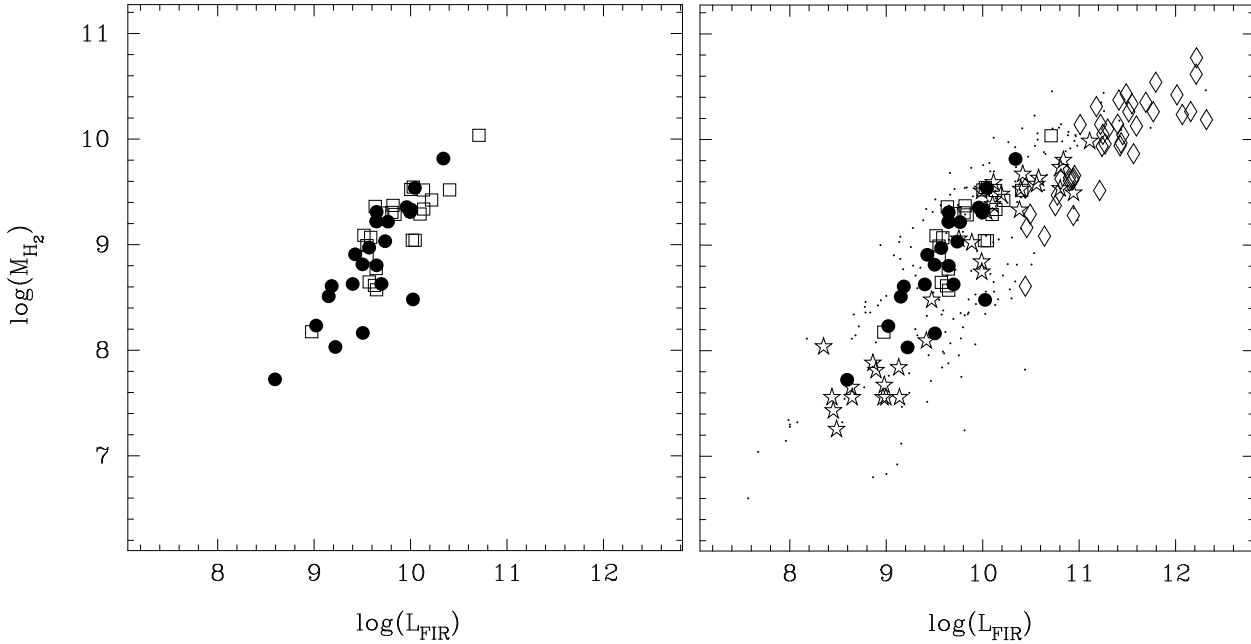


**Fig. 1.** Left panel (a): Total molecular gas as a function of FIR luminosity. The CS is marked by open squares and HDS by filled circles. Right panel (b): The same as in the left panel. Ultraluminous infrared galaxies (Sanders et al. 1991) are marked by open diamonds, normal spiral galaxies from Young et al. (1989) and Braine et al. (1993) are marked by dots, cluster galaxies (Coma and Fornax) from Casoli et al. (1991) and Horellou et al. (1995) are marked by open stars. Luminosity is in  $L_{\odot}$  and mass is in  $M_{\odot}$ .

spectra were extracted of each galaxy integrated along the slit length. We corrected for Galactic extinction using Cardelli et al. (1989) extinction curve and  $E(B-V)$  from NED. All spectra are flux calibrated and corrected for Doppler shift which was calculated using a cross-correlation technique.

Starlight subtraction was particularly critical in weak lines such as  $H\beta$ . The starlight contribution was removed using the technique of McCall, Rybski & Shields (1985, see also Storchi-Bergmann, Calzetti & Kinney 1994). Taking into account that in the typical stellar population the equivalent width of  $H\beta$  in absorption is of the order of  $1.5\text{\AA}$ , we corrected for this effect by adding a factor of 1.5 times the continuum flux around  $H\beta$  to the emission line flux. When no emission line was clearly visible we adopted a theoretical ratio,  $H\alpha/H\beta=2.86$  (Ho et al. 1997). In this case, the value of  $H\beta$  is an upper limit. Therefore, higher ratios of  $H\alpha/H\beta$  can also be expected. We have investigated whether a higher ratio would influence our results by adopting ratios typical of AGNs ( $H\alpha/H\beta=3.1$ ). We found no significant difference given the uncertainties in the continuum determination.

We tested a second method of starlight subtraction using templates of old stellar populations from Bica (1988). We subtracted our spectra from the templates and then measured the fluxes. Both methods gave similar results given the accuracy of the measurements, dominated by

the uncertainty in the continuum determination (Cid Fernandes et al. 1998).

We measured the integrated fluxes and equivalent widths of the emission lines  $H\beta$ ,  $[\text{OIII}]\lambda 5007$ ,  $[\text{NII}]\lambda 6548$ ,  $H\alpha$ ,  $[\text{NII}]\lambda 6583$ ,  $[\text{SII}]\lambda 6716, 6731$  for 35 galaxies with good signal-to-noise spectra. Internal reddening was estimated from Cardelli et al. (1989) extinction curve and  $H\alpha/H\beta$  ratios.  $H\alpha$  equivalent width was measured after internal reddening correction, following the same procedure as in Ho et al. (1997).

The type of activity was classified by measuring line-intensity ratios ( $\log([\text{OIII}]\lambda 5007/H\beta)$  and  $\log([\text{NII}]\lambda 6583/H\alpha)$ ) and applying standard diagnostic diagrams (Baldwin et al. 1981, Veilleux & Osterbrock 1987). In Paper II we show the diagnostic diagram used to classify the type of activity.

Table 2 lists the emission line parameters as follows. Column (1): designation in the ESO-Uppsala catalog (LV89); column (2): type of sample (control sample=CS and high density sample=HDS) and morphological type (LV89) 1=Sa, 2=Sa-b, 3=Sb, 4=Sb-c, 5=S..., 6=Sc, Sc-d, 7=S../Irr, 8=Sd; column (3):  $H\beta$  flux; column (4):  $[\text{OIII}]\lambda 5007$  flux; column (5):  $H\alpha$  flux; column (6):  $[\text{NII}]\lambda 6583$  flux; column (7):  $H\alpha$  equivalent width in  $\text{\AA}$ , and column (8): type of activity (L=LINERS, HII=HII region).

In Appendix A (available at the following webpage <http://www.oso.chalmers.se/~duilia/env.html>) we show

the optical spectra of 35 galaxies of our sample. We also included in the Appendix the CO spectra described below and images from The Digitized Sky Surveys<sup>1</sup> which allows direct inspection of the galaxies morphology.

#### 4. The CO Data

Millimetric observations were carried out at the Swedish-ESO (SEST) 15m radiotelescope at La Silla in October 1996 and September 1998 during good weather conditions. In the first run we used the SESIS 100 receiver with a 1 GHz bandwidth at 115 GHz ( $^{12}\text{CO} (1 - 0)$ ). Typical system temperatures were  $\sim 250$  K (in the  $T_A^*$  scale) at the elevation of the sources and typical zenith opacities between 0.1-0.2. During the second run we used the IRAM 115 and IRAM 230 receivers with 500 MHz and 1 GHz bandwidth, at 115 GHz ( $^{12}\text{CO} (1 - 0)$ ) and 230 GHz ( $^{12}\text{CO} (2 - 1)$ ), respectively. The half power beamwidth of the SEST at 115 GHz is  $45''$  and  $23''$  at 230 GHz.

All galaxies were observed at the central optical coordinate. Integration times were 2–3 hours depending on the signal-to-noise achieved. The pointing was regularly checked on nearby SiO masers. The pointing uncertainties were of the order of  $5''$ . CO emission was detected in 47 galaxies and had low signal-to-noise detection in only 5 galaxies, eso-lv1080110 (HDS), eso-lv1880170 (CS), eso-lv2850050 (HDS), eso-lv3550300 (CS), and eso-lv6050070 (CS). We have not included these galaxies in our analysis.

Two galaxies, eso-lv3470340 and eso-lv4060250, were considerably larger than the SEST beam and were observed in 5 and 7 positions, respectively, spaced by half of a beamwidth ( $23''$ ). In Appendix A (available at <http://www.oso.chalmers.se/~duilia/env.html>) we show each position along the major axis of the galaxy and give their spectra. We have added the intensities at each position in order to obtain the total CO intensity of each galaxy.

The CO spectra were reduced with the CLASS package (Forveille et al. 1990). We have binned the spectra with a boxcar function. Spectra were corrected for first order baseline in most of the cases or third order in a few obvious cases where first order did not give a good fit to the data. CO intensities were calculated by using the main-beam efficiency,  $\eta_{mb}$ , values of 0.7 and 0.5 for 115 GHz and 230 GHz, respectively. We estimated the  $1\sigma$  uncertainty in the integrated line intensity taking into account the channel-to-channel noise (rms), the width of the emission profile ( $\Delta V$ ) and the number of channels (N) that the emission profile covers (error =  $\text{rms} \times \Delta V \times N^{-1/2}$ ).

Table 3 lists the CO data as follows. Column (1): designation in the ESO-Uppsala catalog (LV89); column (2): type of sample (control sample=CS and high density sample=HDS) and morphological type (LV89) 1=Sa, 2=Sa-b,

<sup>1</sup> The Digitized Sky Surveys were produced at the Space Telescope Science Institute under U.S. Government grant NAG W-2166

**Table 4.** CO data from the literature

ESO-LV name	Sample	$I_{\text{CO}(1-0)}$ K kms <sup>-1</sup>	References
1060120	CS	2.2	Combes et al. 1994 <sup>†</sup>
1570050	HDS	<1.2	Horellou & Booth 1997 <sup>†</sup>
3570190	HDS	<0.6	Horellou & Booth 1997 <sup>†</sup>
4780060	CS	5.4±1.8	Andreani et al. 1995 <sup>†</sup>
4840250	CS	3.5±0.7	Andreani et al. 1995 <sup>†</sup>
5450110	HDS	12.2±0.8	Elfhag et al. 1996 <sup>‡</sup>
5480380	HDS	4.4	Combes et al. 1994 <sup>†</sup>

<sup>†</sup> using SEST, <sup>‡</sup> using Onsala 20m

3=Sb, 4=Sb-c, 5=S..., 6=Sc, Sc-d, 7=S./Irr, 8=Sd; column (3): velocity derived from central CO (1 - 0) profiles in kms<sup>-1</sup>; column (4): the width of the emission profile in kms<sup>-1</sup>; column (5): blue luminosity in  $L_{\odot}$  derived from  $B_T$  magnitude (errors in  $L_B$  are within 10% when the magnitude estimates in the RC3 have errors of 0.1mag); column (6): Far-Infrared luminosity in  $L_{\odot}$  calculated as described in the next Section; column (7): CO intensity in the line  $J=(1 - 0)$  in K kms<sup>-1</sup> and errors; column (8):  $\text{H}_2$  masses and errors in  $M_{\odot}$  estimated from the velocity integrated CO (1 - 0) emission as described in the next Section, and column (9): CO intensity in the line  $J=(2 - 1)$  in K kms<sup>-1</sup>. Distances were corrected for the Virgocentric flow according to model 3.1 in Aaronson et al. (1982). Hubble constant value of 75 kms<sup>-1</sup>Mpc<sup>-1</sup> was adopted in all calculations.

Table 4 lists the CO intensity in the line  $J=(1 - 0)$  available in the literature for 7 galaxies (4 in the HDS and 3 in the CS). The differences between the fluxes we have measured and the ones obtained previously are due to (i) different sizes of the beam (Elfhag et al. 1996), (ii) baseline adjustments (Combes et al. 1994, Andreani et al. 1995), or short integration time (Horellou & Booth 1997).

#### 5. General Properties

The FIR emission together with the molecular gas provide unique information in terms of fuel and star formation. The FIR luminosity was calculated using the relation (Lonsdale & Helou 1985)

$$L_{\text{FIR}} = 5.9 \times 10^5 D^2 (2.58 \times F_{60} + F_{100})$$

where  $F_{60}$  and  $F_{100}$  are fluxes in Jy at 60 and 100  $\mu\text{m}$  detected by IRAS and D is the distance in Mpc corrected for the Virgo infall.

$\text{H}_2$  masses were estimated from the velocity integrated CO (1 - 0) emission, using a  $N_{\text{H}_2}/I_{\text{CO}}$  conversion ratio of  $3 \times 10^{20}$  cm<sup>-2</sup> (K kms<sup>-1</sup>).

We are assuming that the conversion factor is the same in all galaxies in our sample. This assumption is reasonable since our sample do not contain any later-type systems (Sd, Sm, Ir) which, despite the ongoing star formation, show weak CO emission (e.g. Rubio et al. 1991).

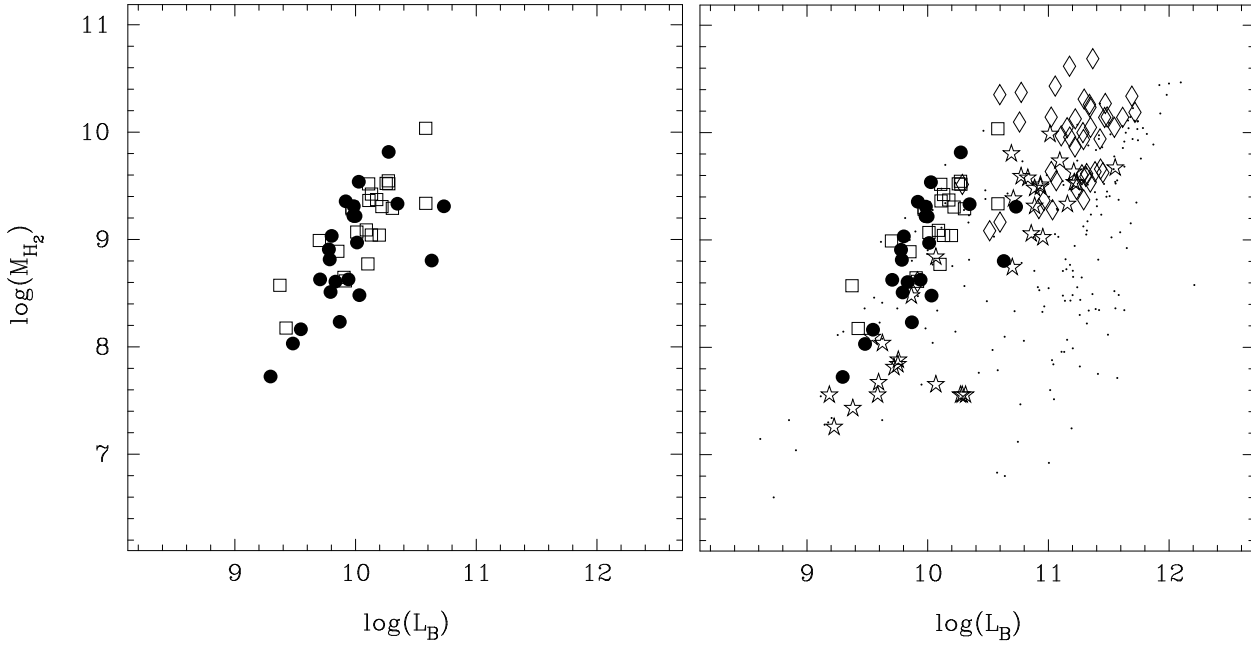


**Fig. 2.** Left panel (a): Total molecular gas as a function of blue luminosity. Right panel (b): The same as in the left panel. Additional samples of ultraluminous infrared galaxies, galaxies in clusters, and spiral galaxies are included. Symbols are the same as in Fig. 1. Luminosity is in  $L_{\odot}$  and mass is in  $M_{\odot}$ .

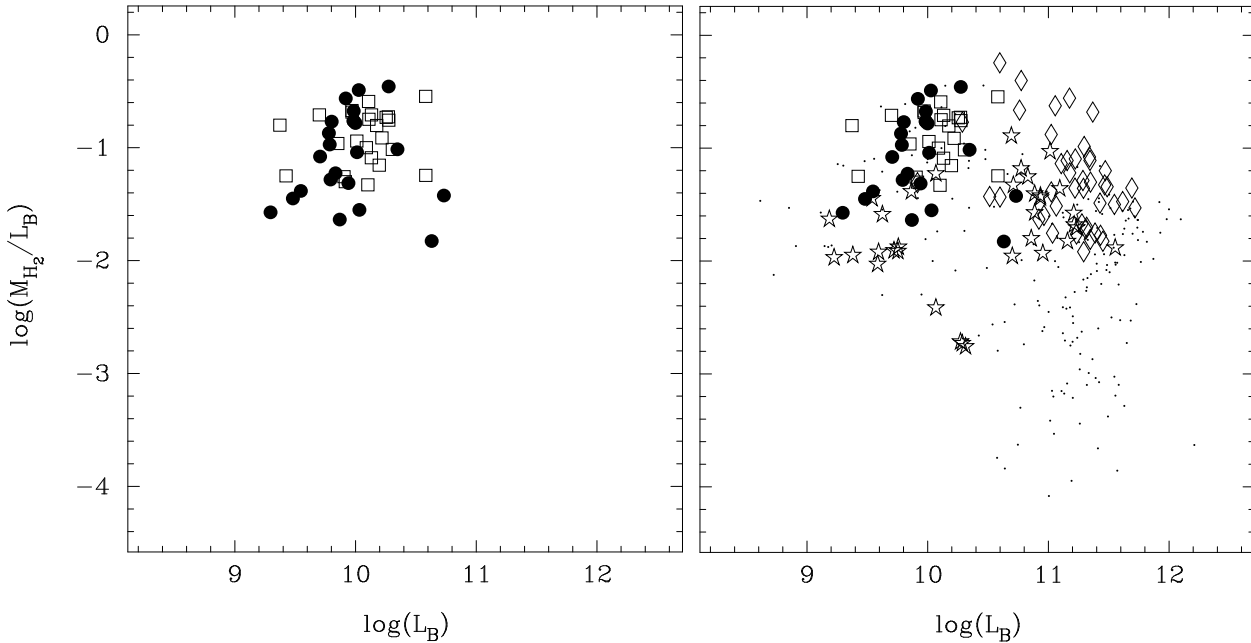


**Fig. 3.** Left panel (a): total molecular gas normalized by the blue luminosity as a function of blue luminosity. Right panel (b): The same as in the left panel. Additional samples of ultraluminous infrared galaxies, galaxies in clusters, and spiral galaxies are included. Symbols are the same as in Fig. 1. Luminosity is in  $L_{\odot}$  and mass is in  $M_{\odot}$ .

Average and median values of  $L_B$ ,  $L_{FIR}$ ,  $M_{H_2}$ , and  $H\alpha$  equivalent width are presented in Table 5.

Fig. 1a and Fig. 2a show the total amount of molecular gas as a function of FIR and blue luminosities. Fig. 1a confirms the known correlation between  $L_{FIR}$  and the  $H_2$

masses (correlation coefficient= 0.80 and 0.84 for the HDS and CS, respectively). From Fig. 2a we verify that galaxies in the CS are on average more luminous than those in the HDS (a distance bias in our subsample). In order to eliminate this effect, CO intensities were normalized by

the blue luminosity,  $L_B$ , in the analysis presented in Paper II. Given our morphological selection criteria, we assumed that the mass/ $L_B$  ratio is approximately the same for our galaxies (Roberts & Haynes 1994) and  $L_B$  is thus a measure of the total mass.

We have plotted the  $M_{H_2}/L_B$  as a function of  $L_B$  (Fig. 3a) in order to compare whether the bias in blue luminosity present in our subsample may cause a bias in our analysis. The correlation found for HDS and CS is very similar (correlation coefficient = -0.03 and 0.06 for the HDS and CS, respectively) suggesting no evident bias. We have compared our sample properties with samples observed by others, such as normal spiral galaxies (Young et al. 1989, Braine et al. 1993), the ultraluminous FIR galaxies (Sanders et al. 1991), and galaxies in the Coma and Fornax clusters (Casoli et al. 1991 and Horellou et al. 1995). As it is shown in Fig. 1b, Fig. 2b, and Fig. 3b the 47 spiral galaxies of our sample (HDS and CS) have correlations between global parameters which are similar to those in other samples. The ultraluminous FIR galaxies (Sanders & Mirabel 1996), as expected, are overall brighter and more massive than our subsample. The other samples include spirals of all types which explains the large dispersion found in luminosities and masses.

As previously mentioned, only intermediate Hubble types (Sb, Sbc, and Sc) were selected in order to avoid any bias due to the correlation between general properties and morphology. However, even in this sample the uncertainties in morphological classification should be taken into account when making any firm statement. Galaxies in dense environments can have their morphology distorted by tidal effects which makes them difficult to classify. One should refer to Appendix A (available at <http://www.oso.chalmers.se/~duilia/env.html>) in order to visually check the morphology of each individual galaxy in more detail. We also refer to the detailed morphological classification taken from RC3 presented on Table 1 which gives a general idea on the complexity of the morphologies.

In Table 3 we give both the CO(1 - 0) and CO(2 - 1) integrated line intensities. In order to estimate the CO(2 - 1)/CO(1 - 0) intensity ratios we need to convolve the CO(2 - 1) data to the same angular resolution as the CO(1 - 0) data. Since we observed only a single position for most galaxies, we can not do this. However, taking the values in Table 3 at face value, the average CO(1 - 0) to CO(2 - 1) line intensity ratio is  $0.93 \pm 0.47$ . This is an upper limit to the line ratio. In the case of a molecular gas distribution more extended than both the CO(1 - 0) and CO(2 - 1) telescope beams (45'' and 23'', respectively), the correction for different angular resolutions would be 1.0. In the other extreme, with the CO emission originating in a point source, the correction for different angular resolutions would be 0.25. Since our telescope beam in almost all cases is large with respect to the optical extent of the galaxies, and since the molecular gas is likely to be

centrally concentrated, the correction for different angular resolutions should be  $\sim 0.5$ . Our average line ratio is thus  $\sim 0.5 \pm 0.4$ . This value is lower than that found by Braine et al. (1993) of  $0.89 \pm 0.34$  for normal spiral galaxies. The lower value is characteristic of optically thick and subthermally excited molecular gas and most likely reflects the lower star formation activity in our environmentally selected sample as opposed to far infrared bright selected samples.

In Fig. 4 we verify that the HDS and CS are also very similar to the galaxies in other samples in terms of SFE. We conclude that the intermediate type spirals in the HDS and CS do not belong to a separate class of object but contain objects with properties similar to galaxies in clusters, nearby spiral galaxies and infrared luminous galaxies.

## 6. Summary

In this paper we present millimetric and optical data obtained in order to study environmental effects in galaxies. Our sample has 47 intermediate Hubble type spirals in either dense environments or in the field. We compared general properties, such as far-infrared luminosity, blue luminosity, and total molecular gas content, to other samples of galaxies, such as ultraluminous infrared galaxies, clusters of galaxies and spiral galaxies. We find that overall our sample has general properties very similar to these other galaxies; i.e. they are not a separate class of objects.

*Acknowledgements.* The ON team of observers at the ESO1.52m, in particular Christopher Willmer for helping with the data reduction. Henrique Schmitt for valuable suggestions regarding the stellar contamination. This research has made use of the NASA/IPAC Extragalactic Database (NED) which is operated by the Jet Propulsion Laboratory, California Institute of Technology, under contract with the National Aeronautics and Space Administration. The Digitized Sky Surveys were produced at the Space Telescope Science Institute under U.S. Government grant NAG W-2166. The images of these surveys are based on photographic data obtained using the Oschin Schmidt Telescope on Palomar Mountain and the UK Schmidt Telescope. D.F.M. was partially supported by CNPq Fellowship 301456/95-0, and the Swedish *Vetenskapsrådet* project number F620-489/2000. M.A.G.M. was supported by CNPq grant 301366/86-1. T.W. was supported by *Vetenskapsrådet* project number F1299/1999.

## References

- Aaronson, M., Huchra, J., Mould, J., Schechter, P.L., & Tully, R.B. 1982, ApJ 258, 64
- Andreani, P., Casoli, F., Gerin, M. 1995, A&A, 300, 43
- Baldwin, J.A., Phillips, M.M., & Terlevich, R. 1981, PASP 93, 5
- Bica, E. 1988, A&A 195, 76
- Braine, J., Combes, F., Casoli, F., Dupraz, C., Gerin, M., Klein, U., Wielebinski, R., & Brouillet, N. 1993, A&AS 97, 88

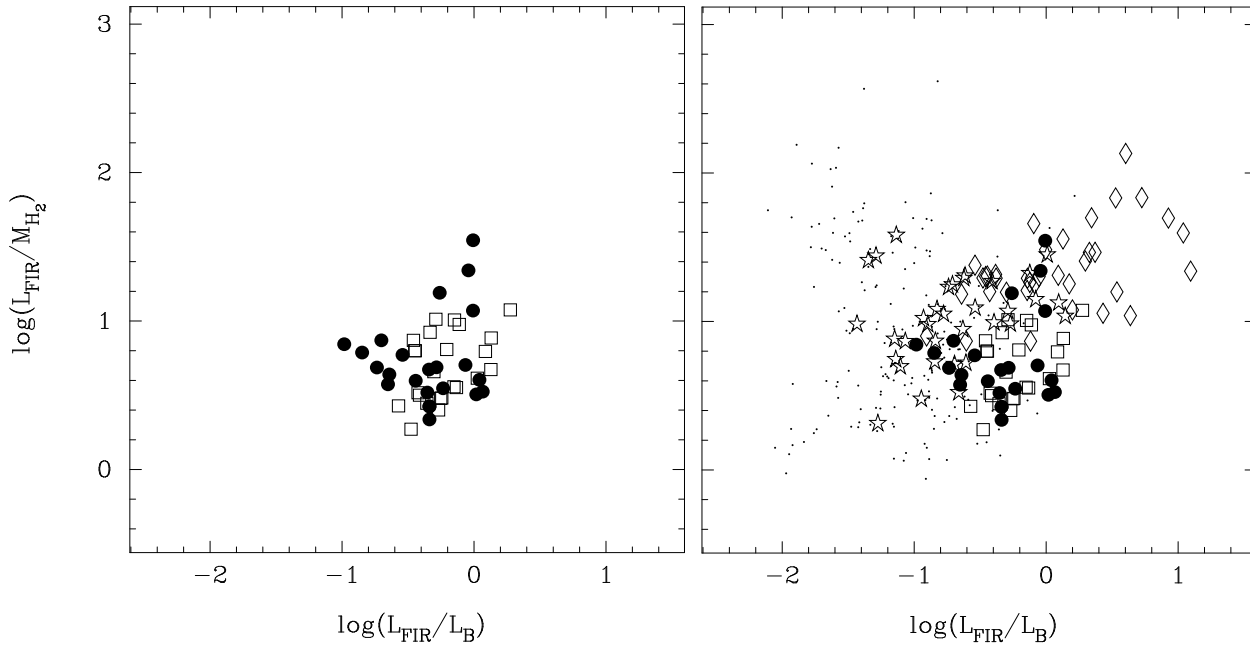


**Fig. 4.** Left panel (a): FIR luminosity normalized by the total molecular gas as a function of the FIR luminosity normalized by the blue luminosity. Right panel (b): The same as in the left panel. Additional samples of ultraluminous infrared galaxies, galaxies in clusters, and spiral galaxies are included. Symbols are the same as in Fig. 1. Luminosity is in  $L_{\odot}$  and mass is in  $M_{\odot}$ .

- Cardelli, J.A., Clayton, G.C., & Mathis, J.S. 1989, *ApJ* 345, 245
- Casoli, F., Boisse, P., Combes, F., & Dupraz, C. 1991, *A&A* 249, 359
- Casoli, F., Sauty, S., Gerin, M., Boselli, A., Fouque, P., Braine, J., Gavazzi, G., Lequeux, J., & Dickey, J. 1998, *A&A* 331, 451
- Cid Fernandes, R.Jr., Storchi-Bergmann, T., & Schmitt, H.R. 1998, *MNRAS* 297, 579
- Combes, F., Prugniel, P., Rampazzo, R., & Sulentic, J.W. 1994, *A&A* 281, 725
- Coziol, R., Iovino, A., & de Carvalho, R.R. 2000, *AJ* 120, 47
- da Costa, L.N., Pellegrini, P.S., Willmer, C., de Carvalho, R., Maia, M., Latham, D.W., & Geary, J.C. 1989, *AJ* 97, 315
- de Mello, D.F., Wiklind, T., Maia, M.A.G. 2001, *A&A* submitted (Paper II)
- de Vaucouleurs, G., de Vaucouleurs, A., Corwin, H.G., Jr., Buta, R.J., Paturel, G., & Fouqu, P. 1991, *Third Reference Catalogue of Bright Galaxies (RC3)* (New York: Springer)
- Dressler, A. 1980, *ApJ* 236, 351
- Elfhag, T. Booth, R.S., Hoeglund, B., Johansson, L.E.B., & Sandqvist, A. 1996, *A&AS* 115, 439
- Forveille, T., Guilloteau, S., & Lucas, R. 1990, IRAM internal report
- Hickson, P. 1982, *ApJ* 255, 382
- Ho, L.C., Filippenko, A.V., Sargent, W.L.W. 1997, *ApJ* 112, 315
- Horellou, C., Casoli, F., Combes, F., & Dupraz, C. 1995, *A&A* 298, 743
- Horellou, C., & Booth, R. 1997, *A&AS* 126, 3
- Huchra, J. P., & Geller, M.J. 1982, *ApJ* 257, 423
- Lauberts, A. 1982, *The ESO/Uppsala Survey of the ESO(B) Atlas* (Munich: European Southern Observatory)
- Lauberts, A., & Valentijn, E.A. 1989, *The Surface Photometry Catalogue of the ESO-Uppsala Galaxies* (Garching bei München: ESO)
- Leon, S., Combes, F., & Menon, T.K. 1998, *AA*, 330, 37
- Liu, C.T., & Kennicutt, R.C.Jr. 1995, *ApJ* 450, 547
- Lonsdale, C., & Helou, G. 1985, *Cataloged galaxies and quasars observed in the IRAS survey*. Pasadena: Jet Propulsion Laboratory (JPL)
- Maia, M.A.G., da Costa, L.N., & Latham, D.W. 1989, *ApJS* 69, 809
- Maia, M.A.G., Pastoriza, M.G., Bica, E., Dottori, H. 1994, *ApJSS* 93, 425
- McCall, M.L., Rybski, P.M., & Shields, G.A. 1985, *ApJS* 57, 1
- Moshir, M. et al. 1990, *IRAS Faint Source Catalogue*, version 2.0.
- Roberts, M.S., & Haynes, M.P. 1994, *ARA&A* 32, 115
- Rubio, M., Garay, G., Montani, J., & Thaddeus, P. 1991, *ApJ* 368, 173
- Sage, L.J. 1993, *A&AS*, 100, 537
- Sanders, D.B., Scoville, N.Z., & Soifer, B.T. 1991, *ApJ* 370, 158
- Sanders, D.B., & Mirabel, I.F. 1996, *ARA&A* 34, 749
- Sanroma, M., & Salvador-Solé, E. 1990, *ApJ* 360, 16
- Storchi-Bergmann, T. Calzetti, D., & Kinney, A.L. 1994, *ApJ* 429, 572
- Young, J.S., Shuding, X., Kenney, J.D.P. et al. 1989, *ApJS* 70, 699
- Veilleux, S., & Osterbrock, D.E. 1987, *ApJS* 63, 295
- Whitmore, B.C., & Gilmore, D.M. 1991, *ApJ* 367, 64
- Willmer, C.N.A., Maia, M.A.G., Mendes, S.O., Alonso, M.V., Rios, L.A., Chaves, O.L., & de Mello, D. 1999, *AJ* 118, 1131
- Zabludoff, A.I., & Mulchaey, J.S. 1998, *ApJ* 496, 39



**Table 1.** Observed Sample

ESO-LV Name (1)	Other Name (2)	Coord. J2000 (3)	Sample & Morph. (4)	Morph. RC3 (5)	$N_g$ (6)	$r_p$ Mpc (7)	$B_T$ (8)	$F_{60\mu m}$ Jy (9)	$F_{100\mu m}$ Jy (10)
5390050		00 17 10.1 -19 18 00	CS 5	SAB(rs)c?			13.53	0.977	2.972
3500140	N101	00 23 54.6 -32 32 09	CS 6	SAB(rs)c			13.37	0.549	1.754
3520530	N491	01 21 20.3 -34 03 48	HDS 3	SB(rs)b:	3	0.18	13.21	2.843	8.632
2960380		01 32 27.4 -38 40 40	CS 4	SAB(rs)c			13.99	0.516	1.779
4780060		02 09 19.1 -23 24 54	CS 4	Sbc			13.22	3.543	9.112
5450100	N907	02 23 01.7 -20 42 43	HDS 5	SBdm? sp	5	0.40	13.21	2.649	5.625
5450110	N908	02 23 04.8 -21 14 03	HDS 5	SA(s)c			10.83	14.770	43.670
3550260		02 32 17.5 -35 01 50	CS 4	SB(s)bc:			13.80	0.482	1.588
3550300		02 37 36.4 -32 55 28	CS 4	SB(rs:)bc:			13.59	0.881	3.137
0310050		02 58 06.0 -74 27 24	CS 3.5	SAB(rs)bc			14.07	1.043	3.887
3570190	N1310	03 21 03.7 -37 05 58	HDS 5	SB(rs)cd	55	0.82	12.55	0.881	3.345
5480070	N1325	03 24 25.6 -21 32 35	HDS 3.5	SA(s)bc	7	0.94	12.22	0.631	3.211
5480310	N1353	03 32 03.0 -20 49 04	HDS 3	SA(rs)bc	7	0.94	12.40	2.420	8.786
5480380	I1953	03 33 41.7 -21 28 45	HDS 6	SB(rs)d	7	0.94	12.24	8.470	11.128
4190030		03 42 11.2 -27 51 47	CS 4	(R')SAB(rs)c			13.60	1.334	3.361
4820430	N1459	03 46 58.0 -25 31 11	CS 4	SB(s)bc?			13.62	0.572	2.657
4200030		04 07 45.8 -29 51 30	CS 5	SA(rs)bc			13.52	0.704	2.172
2010220		04 08 59.3 -48 43 42	CS 5	Sbc			14.73	0.356	1.466
1570050	N1536	04 10 59.9 -56 28 48	HDS 5.5	SB(s)c pec:	46	1.30	13.15	0.475	1.649
4840250	N1591	04 29 30.7 -26 42 44	CS 2	SB(r)ab pec			13.77	1.929	5.001
1190060	N1688	04 48 23.8 -59 47 59	HDS 7.5	SB(rs)dm	14	0.85	12.57	2.683	6.677
1190190	N1703	04 52 51.9 -59 44 33	HDS 5	SA(s)c	14	0.85	11.90	2.122	7.723
3050140		05 12 34.1 -39 51 36	CS 5	SB(s)c			14.13	0.378	0.982
2030180	N1803	05 05 26.6 -49 34 05	CS 4	Sbc:			13.38	0.277	0.715
1420500	I4901	19 54 23.1 -58 42 50	CS 5	SAB(r)c			12.29	1.778	6.518
2340160		20 23 25.1 -50 32 43	HDS 5	SAB(s)bc pec	4	0.68	14.56	3.069	7.875
2850080	N6902	20 24 27.7 -43 39 09	HDS 4	SA(r)b	4	0.31	11.64	0.826	3.924
1060120	I5038	20 46 51.2 -65 01 00	CS 6	(R')SB(s)bc			14.13	0.723	2.460
2350550		21 05 55.4 -48 12 23	HDS 5	(R')SAB(rs)bc	9	1.00	12.70	0.461	2.840
2350570		21 06 21.8 -48 10 14	HDS 4	Sbc: sp	9	1.00	14.45	0.461	3.368
2860820		21 15 45.4 -42 25 33	HDS 5	SAB(s)c	3	0.20	14.51	0.337	1.032
2370020	N7124	21 48 05.7 -50 33 51	CS 4.5	SB(rs)c			13.10	0.791	3.411
1890070	N7140	21 52 15.3 -55 34 10	CS 4	(R')SB(rs)b			12.20	2.183	5.886
2880260	N7162	21 59 39.0 -43 18 12	HDS 5	(R')SA(r)bc	4	0.20	13.29	0.484	1.656
5320090	N7167	22 00 30.9 -24 38 00	CS 5	SB(s)c:			13.22	1.314	3.588
6010040		22 01 30.4 -22 04 15	CS 4.6	SB(s)c:			14.58	0.227	0.877
1080130	N7191	22 06 51.3 -64 38 03	HDS 3.5	SAB(rs)c	5	0.48	13.80	0.570	2.061
1080200	I5176	22 11 55.0 -66 50 46	CS 3.9	SAB(s)bc?sp			13.54	3.031	11.21
1460090	N7205	22 08 34.4 -57 26 33	CS 5	SA(s)bc			11.55	8.861	25.960
4050180	N7267	22 24 21.6 -33 41 38	CS 1	(R')SB(rs)a			12.91	2.081	4.930
4060250	N7418	22 56 36.0 -37 01 47	HDS 5	SAB(rs)cd	32	1.31	11.66	4.344	15.010
4060330	I5270	22 57 54.7 -35 51 30	HDS 6	SB(rs)c	32	1.31	13.00	3.076	8.398
4070140		23 17 39.7 -34 47 24	CS 5	SB(s)c?			13.48	0.987	2.766
3470340	N7599	23 19 21.1 -42 15 20	HDS 3	SB(s)c	32	1.31	12.08	5.408	21.750
2400110		23 37 49.7 -47 43 42	HDS 4.8	Sb	3	0.18	13.20	0.956	5.612
2400130		23 39 26.9 -47 46 27	HDS 3	(R')SAB(rs)b	3	0.18	13.99	0.791	3.411
4710200	N7755	23 45 51.8 -30 31 19	CS 4.5	SB(r)bc			12.56	2.686	8.538

Column(4): CS=control sample, HDS=high density sample; morphological types are: 1=Sa, 2=Sa-b, 3=Sb, 4=Sb-c, 5=S..., 6=Sc, Sc-d, 7=S../Irr, 8=Sd. Column(6):  $N_g$  is the number of companions from Maia et al. 1989. Column(7):  $r_p$  is the mean pairwise separation from Maia et al. 1989.

**Table 2.** Parameters of Strong Emission Lines

ESO-LV name (1)	Sample & Morph. (2)	$F(\text{H}\beta) \times 10^{-15}$ ergs $\text{cm}^{-2} \text{s}^{-1}$ (3)	$F([\text{OIII}]5007) \times 10^{-15}$ ergs $\text{cm}^{-2} \text{s}^{-1}$ (4)	$F(\text{H}\alpha) \times 10^{-15}$ ergs $\text{cm}^{-2} \text{s}^{-1}$ (5)	$F([\text{NII}]6583) \times 10^{-15}$ ergs $\text{cm}^{-2} \text{s}^{-1}$ (6)	$\text{EW}(\text{H}\alpha)$ $\text{\AA}$ (7) <sup>†</sup>	Type of Activity (8)
0310050	CS 3.5	4.0	0.3	15.0	8.2	8.2	HII
1060120	CS 6	10.2	1.5	38.0	18.0	12.4	HII
1080130	HDS 3.5	7.2	0.6	41.0	15.0	14.2	HII
1190190	HDS 5	5.7	1.3	12.0	6.7	5.5	HII
1420500	CS 5	10.0	2.8	20.0	16.0	3.0	L
1460090	CS 5	21.0	5.1	60.0	31.0	5.6	HII
1570050	HDS 5.5	14.5	4.4	53.0	17.0	27.9	HII
2010220	CS 5	12.0	8.8	45.8	13.1	16.6	HII
2030180	CS 4	45.4	23.3	160	63.0	29.2	HII
2340160	HDS 5	11.6	8.0	40.0	15.0	29.6	HII
2350550	HDS 5	3.0	2.4	8.7	17.0		L
2350570	HDS 4	2.1	2.7	5.9	11.0	1.2	L
2370020	CS 4.5	7.9	2.8	3.3	9.5	0.9	L
2400110	HDS 4.8	12.0	0.9	16.6	18.5	1.9	L
2850080	HDS 4	14.6	4.2	9.0	17.0	1.1	L
2860820	HDS 5	8.0	0.9	27.0	11.0	14.6	HII
2880260	HDS 5	19.0	1.0	49.0	32.0	6.6	L
2960380	CS 4	7.2	1.7	26.0	10.0	16.5	HII
3050140	CS 5	1.8	0.4	6.7	3.8	8.7	HII
3500140	CS 6	8.7	2.6	33.0	14.0	13.3	HII
3550300	CS 4	12.2	2.6	22.2	18.0	3.7	L
3570190	HDS 5	13.4	8.4	50.0	22.0	14.9	HII
4060330	HDS 6	43.0	21.0	180	66.0	27.4	HII
4070140	CS 5	53.2	51.0	190	58.0	40.6	HII
4190030	CS 4	5.1	1.6	22.0	7.8	24.2	HII
4200030	CS 5	15.2	4.7	48.0	18.0	13.3	HII
4710200	CS 4.5	24.3	6.5	98.0	47.0	10.3	HII
4780060	CS 4	23.1	6.0	63.0	26.0	13.7	HII
4820430	CS 4	6.9	2.6	17.0	9.4	6.7	HII
5320090	CS 5	16.8	7.3	51.0	21.0	13.4	HII
5390050	CS 5	16.7	9.2	64.0	28.0	20.0	HII
5450100	HDS 5	23.4	24.7	95.0	26.0	30.0	HII
5480310	HDS 3	16.0	1.0	53.0	35.0	4.2	L
5480380	HDS 6	5.6	1.4	24.0	9.6	28.8	HII
6010040	CS 4.6	8.6	1.0	30.0	14.0	6.6	HII

Column (2): CS=control sample, HDS=high density sample; morphological types are: 1=Sa, 2=Sa-b, 3=Sb, 4=Sb-c, 5=S..., 6=Sc, Sc-d, 7=S../Irr, 8=Sd. Column (8): HII=activity typical of HII regions, L=activity typical of LINERs.

<sup>†</sup> Only  $\text{EW}(\text{H}\alpha)$  is corrected for internal reddening.

**Table 3.** CO Data

ESO-LV name (1)	Sample & Morph. (2)	$V_{CO}$ $\text{kms}^{-1}$ (3)	$\Delta V_{CO}$ $\text{kms}^{-1}$ (4)	$\log L_B$ $L_\odot$ (5)	$L_{FIR} \times 10^9$ $L_\odot$ (6)	$I_{CO(1-0)}$ $\text{K kms}^{-1}$ (7)	$M_{H_2} \times 10^9$ $M_\odot$ (8)	$I_{CO(2-1)}$ $\text{K kms}^{-1}$
0310050	CS 3.5	4714	287	10.11	$13.60 \pm 0.39$	$3.62 \pm 0.26$	$3.30 \pm 0.23$	$3.64 \pm 0.22$
1060120	CS 6	4154	180	9.97	$6.90 \pm 0.39$	$2.75 \pm 0.28$	$1.93 \pm 0.19$	
1080130	HDS 3.5	2941	135	9.78	$2.67 \pm 0.15$	$2.43 \pm 0.21$	$0.81 \pm 0.07$	
1080200	CS 3.9	1720	183	9.37	$4.45 \pm 0.20$	$6.28 \pm 0.25$	$0.65 \pm 0.03$	$3.63 \pm 0.18$
1190060	HDS 7.5	1256	43	9.48	$1.66 \pm 0.05$	$1.99 \pm 0.14$	$0.11 \pm 0.01$	
1190190	HDS 5	1527	33	9.94	$2.52 \pm 0.07$	$5.06 \pm 0.19$	$0.42 \pm 0.02$	
1420500	CS 5	2135	165	10.10	$4.40 \pm 0.09$	$3.40 \pm 0.25$	$0.59 \pm 0.04$	
1460090	CS 5	1652	183	10.13	$10.40 \pm 0.34$	$11.68 \pm 0.66$	$1.10 \pm 0.06$	
1570050	HDS 5.5	1311	40	9.30	$0.39 \pm 0.02$	$1.66 \pm 0.06$	$0.10 \pm 0.01$	$0.88 \pm 0.09$
1890070	CS 4.0	3006	169	10.44	$9.15 \pm 0.36$	$4.22 \pm 0.26$	$1.48 \pm 0.09$	
2010220	CS 5	3990	188	9.70	$3.53 \pm 0.23$	$1.50 \pm 0.11$	$0.98 \pm 0.07$	$1.30 \pm 0.11$
2030180	CS 4	4123	157	10.27	$25.39 \pm 1.17$	$4.66 \pm 0.23$	$3.30 \pm 0.16$	$5.04 \pm 0.14$
2340160	HDS 5	5218	10	10.01	$3.72 \pm 0.50$	$0.82 \pm 0.05$	$0.94 \pm 0.06$	$0.45 \pm 0.12$
2350550	HDS 5	5098	70	10.73	$9.92 \pm 1.11$	$1.88 \pm 0.11$	$2.04 \pm 0.12$	$1.34 \pm 0.11$
2350570	HDS 4	5069	248	10.03	$11.08 \pm 1.30$	$3.22 \pm 0.12$	$3.45 \pm 0.13$	$3.56 \pm 0.22$
2370020	CS 4.5	5214	236	10.58	$13.72 \pm 0.70$	$4.42 \pm 0.16$	$4.90 \pm 0.18$	$1.96 \pm 0.11$
2400110	HDS 4.8	2890	278	10.00	$5.81 \pm 0.31$	$5.20 \pm 0.17$	$1.65 \pm 0.05$	
2400130	HDS 3	3284	50	9.80	$5.17 \pm 0.31$	$2.58 \pm 0.15$	$1.08 \pm 0.06$	
2850080	HDS 4	2838	132	10.63	$4.45 \pm 0.23$	$1.97 \pm 0.21$	$0.64 \pm 0.07$	
2860820	HDS 5	4958	134	9.98	$4.42 \pm 0.51$	$1.62 \pm 0.09$	$1.66 \pm 0.09$	$1.68 \pm 0.08$
2880260	HDS 5	2383	80	9.79	$1.42 \pm 0.10$	$1.51 \pm 0.11$	$0.32 \pm 0.02$	
2960380	CS 4	3645	51	9.90	$3.73 \pm 0.33$	$0.84 \pm 0.12$	$0.44 \pm 0.06$	
3050140	CS 5	4761	450	10.11	$4.31 \pm 0.55$	$2.38 \pm 0.10$	$2.31 \pm 0.10$	$1.21 \pm 0.08$
3470340	HDS 3	1671	117	9.92	$7.85 \pm 0.79$	$23.46^\dagger \pm 0.62$	$2.27 \pm 0.06$	
3500140	CS 6	3400	35	10.09	$3.30 \pm 0.25$	$2.68 \pm 0.09$	$1.23 \pm 0.04$	
3520530	HDS 3	3874	260	10.27	$21.89 \pm 0.93$	$10.85 \pm 0.52$	$6.55 \pm 0.32$	
3550260	CS 4	1985	105	9.42	$0.95 \pm 0.07$	$1.02 \pm 0.13$	$0.15 \pm 0.02$	
3550300	CS 4	4448	336	10.25	$10.05 \pm 0.43$	$4.08 \pm 0.44$	$3.33 \pm 0.36$	
3570190	HDS 5	1789	66	9.83	$1.52 \pm 0.06$	$3.40 \pm 0.28$	$0.41 \pm 0.03$	
4050180	CS 1	3375	124	10.27	$10.67 \pm 0.68$	$7.70 \pm 0.37$	$3.52 \pm 0.17$	
4060250	HDS 5	1470	83	9.98	$4.42 \pm 0.20$	$27.44^\ddagger \pm 0.74$	$2.04 \pm 0.05$	
4060330	HDS 6	1922	110	9.71	$5.01 \pm 0.21$	$3.15 \pm 0.17$	$0.42 \pm 0.02$	
4070140	CS 5	2761	129	9.85	$3.54 \pm 0.23$	$2.64 \pm 0.14$	$0.78 \pm 0.04$	
4190030	CS 4	4146	83	10.20	$11.19 \pm 0.36$	$1.52 \pm 0.13$	$1.10 \pm 0.09$	
4200030	CS 5	4093	163	10.22	$6.41 \pm 0.41$	$2.86 \pm 0.20$	$2.02 \pm 0.14$	
4710200	CS 4.5	3017	160	10.30	$12.49 \pm 0.53$	$5.46 \pm 0.36$	$1.95 \pm 0.13$	
4780060	CS 4	5401	164	10.58	$51.12 \pm 2.91$	$8.79 \pm 0.37$	$10.86 \pm 0.46$	$15.16 \pm 0.33$
4820430	CS 4	4073	85	10.17	$6.57 \pm 0.33$	$3.36 \pm 0.30$	$2.35 \pm 0.21$	
4840250	CS 2	4128	191	10.13	$16.54 \pm 0.64$	$3.63 \pm 0.31$	$2.65 \pm 0.22$	
5320090	CS 5	2582	83	9.91	$4.22 \pm 0.20$	$1.54 \pm 0.17$	$0.41 \pm 0.05$	
5390050	CS 5	3158	256	9.98	$5.03 \pm 0.29$	$4.95 \pm 0.33$	$1.99 \pm 0.13$	
5450100	HDS 5	1715	21	9.55	$3.21 \pm 0.14$	$1.29 \pm 0.09$	$0.15 \pm 0.01$	$2.67 \pm 0.13$
5450110	HDS 5	1456	168	10.35	$14.78 \pm 0.72$	$27.01 \pm 0.92$	$2.15 \pm 0.07$	
5480070	HDS 3.5	1557	17	9.87	$1.05 \pm 0.05$	$1.79 \pm 0.11$	$0.17 \pm 0.01$	
5480310	HDS 3	1531	108	9.79	$3.17 \pm 0.13$	$6.99 \pm 0.32$	$0.65 \pm 0.03$	
5480380	HDS 6	1874	86	10.03	$10.56 \pm 0.31$	$2.14 \pm 0.15$	$0.30 \pm 0.02$	
6010040	CS 4.6	5219	103	10.01	$3.85 \pm 0.56$	$1.01 \pm 0.08$	$1.17 \pm 0.09$	$0.78 \pm 0.04$

<sup>†</sup> added CO(1 – 0) intensities of 5 points (map)

<sup>‡</sup> added CO(1 – 0) intensities of 7 points (map)

Column (2): CS=control sample, HDS=high density sample; morphological types are: 1=Sa, 2=Sa-b, 3=Sb, 4=Sb-c, 5=S..., 6=Sc, Sc-d, 7=S../Irr, 8=Sd.

**Table 5.** Average Values

Sample	$\log L_B$ $L_\odot$	$\log L_{\text{FIR}}$ $L_\odot$	$\log M_{\text{H}_2}$ $M_\odot$	$\text{EW}(\text{H}\alpha)^\dagger$ $\text{\AA}$
HDS mean	$9.94 \pm 0.33$	$9.59 \pm 0.40$	$8.86 \pm 0.39$	$15.9 \pm 11.3$
HDS median	$9.94 \pm 0.12$	$9.65 \pm 0.28$	$8.91 \pm 0.40$	$14.2 \pm 11.2$
CS mean	$10.08 \pm 0.29$	$9.85 \pm 0.35$	$9.18 \pm 0.39$	$8.7 \pm 3.4$
CS median	$10.11 \pm 0.14$	$9.82 \pm 0.21$	$9.29 \pm 0.22$	$8.2 \pm 3.3$

<sup>†</sup> Without LINERs.